Dalton Transactions

ROYAL SOCIETY OF CHEMISTRY

PAPER

View Article Online
View Journal | View Issue

Check for updates

Cite this: *Dalton Trans.*, 2023, **52**, 6934

Synthesis, characterization, and *in vivo* evaluation of the anticancer activity of a series of 5- and 6-(halomethyl)-2,2′-bipyridine rhenium tricarbonyl complexes†

Sara Nasiri Sovari,[a] Isabelle Kolly,[a] Kevin Schindler,[a] Ana Djuric,[b] Tatjana Srdic-Rajic,[b] Aurelien Crochet,[a] Aleksandar Pavic*[c] and Fabio Zobi*[a]

Received 16th December 2022,
Accepted 9th March 2023

DOI: 10.1039/d2dt04041g

rsc.li/dalton

We report the synthesis, characterization, and *in vivo* evaluation of the anticancer activity of a series of 5- and 6-(halomethyl)-2,2′-bipyridine rhenium tricarbonyl complexes. The study was promoted in order to understand if the presence and position of a reactive halomethyl substituent on the diimine ligand system of *fac*-$[Re(CO)_3]^+$ species may be a key molecular feature for the design of active and non-toxic anticancer agents. Only compounds potentially able to undergo ligand-based alkylating reactions show significant antiproliferative activity against colorectal and pancreatic cell lines. Of the new species presented in this study, one compound (5-(chloromethyl)-2,2′-bipyridine derivative) shows significant inhibition of pancreatic tumour growth *in vivo* in zebrafish-Panc-1 xenografts. The complex is noticeably effective at 8 μM concentration, lower than its *in vitro* IC_{50} values, being also capable of inhibiting *in vivo* cancer cells dissemination.

1. Introduction

Cisplatin is well known for being the first metallodrug for treatment of neoplastic diseases,[1] but after gaining clinical success, its use was limited due to the emergence of side effects (*e.g.*, inherent nephrotoxicity and ototoxicity). The discovery of cisplatin, however, ignited a thriving field of research, with several medicinal inorganic chemists now exploring the potential anticancer efficacy of other transition metal species. Classic platinum(II) and new platinum(IV) complexes still dominate the literature[2] with ruthenium, copper and gold being other prominent examples.[3–5] Rhenium(I) tricarbonyl complexes are amongst the least explored in the field, but in the last decade have gained significant attention due to their unique and promising properties, which include high stability, low toxicity and rich spectroscopic and luminescent features. The surprising number of recent reviews[6–15] on the anticancer potential of Re species corroborates the interest around such complexes.

Apart from the constant *fac*-$[Re(CO)_3]^+$ core, little is known about what molecular features may be commonly required for an active compound. An examination of the published contributions in the field, generally indicates that the cytotoxicity of Re(I) tricarbonyl complexes positively correlates with lipophilic properties of the species,[16–20] which is associated with an improved passive cellular uptake. Different Re(I) tricarbonyl molecules possessing neoplastic activities (often with *in vitro* anti-proliferative potency higher than cisplatin[14]) act by different mechanisms of action, including mitochondrial[21–25] or enzymatic inhibition,[26] DNA interaction[27–30] or endoplasmic reticulum (ER) stress.[31] Of the different complexes published to date, a few molecules are, in our view, of particular interest, because they have been studied in more details *in vivo*. These are the tricarbonyl rhenium isonitrile polypyridyl (TRIP) complex of Wilson *et al.*, the diseleno-ether compound of Collery *et al.* (diSe-Re in Chart 1) and the N-heterocylic carbene complex (NHC-Re, Chart 1) of Falasca *et al.*

TRIP exhibits potent *in vitro* anticancer activity in a variety of cell lines (IC_{50} value 1.4–1.9 μM) and acts by triggering the accumulation of misfolded proteins, which causes endoplasmic reticulum (ER) stress, unfolded protein response, and apoptotic cell death in addition to mitochondrial fission.[31]

[a]*Department of Chemistry, University of Fribourg, Chemin du Musée 10, 1700 Fribourg, Switzerland. E-mail: fabio.zobi@unifr.ch; Fax: (+41) 26 300 97 37; Tel: (+41) 26 300 87 85*
[b]*Department of experimental oncology, Institute for Oncology and Radiology of Serbia, Pasterova 14, Beograd, Republic of Serbia*
[c]*Institute of Molecular Genetics and Genetic Engineering, University of Belgrade, Vojvode Stepe 444a, 11000 Belgrade, Republic of Serbia. E-mail: sasapavic@imgge.bg.ac.rs; Fax: (+381) 11 397 58 08; Tel: (+381) 11 397 60 34*

† Electronic supplementary information (ESI) available. CCDC 2090791–2090797. For ESI and crystallographic data in CIF or other electronic format see DOI: https://doi.org/10.1039/d2dt04041g

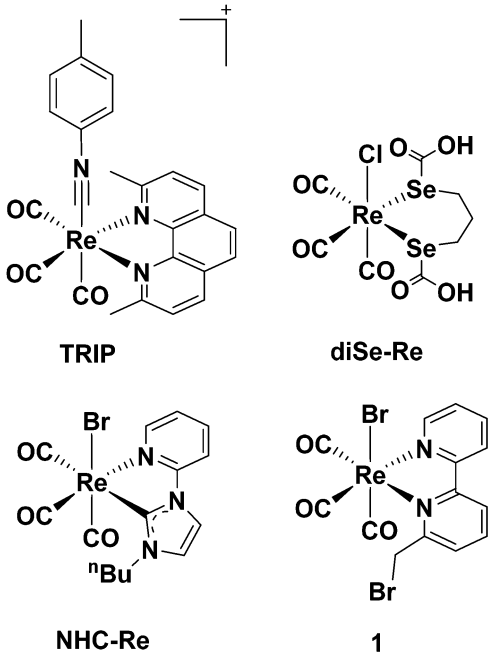

Chart 1 Selected structures of anticancer Re complexes evaluated *in vivo*.

The compound remains intact *in vitro* as demonstrated by X-ray fluorescence microscopy (XFM),[32] and when administered in NSG mice bearing A2780 ovarian cancer xenografts (20 mg per kg twice weekly), it is able to inhibit tumor growth and prolong mouse survival by 150% compared to control.[33] DiSe-Re exhibits activities against several solid tumor cell lines[34] and a potent inhibitory effect on breast cancer MDA-MB231 cell division.[35] Moreover, diSe-Re promotes *in vivo* (10 mg kg^{-1} d^{-1}) a remarkable reduction of tumors volume in mice-bearing a MDA-MB231 Luc+ xenografts and pulmonary metastases without signs of clinical toxicity.[35] The compound acts as an anti-oxidant agent (decreasing ROS production) and significantly decreases the levels of the transforming growth factor beta 1 (TGF-β1), vascular endothelial growth factor A (VEGF-A) and insulin-like growth factor 1 (IGF-1).[36,37] NHC-Re shows low μM activity against pancreatic cancer cell lines where it induces cell cycle arrest at the G2/M phase by inhibiting the phosphorylation of Aurora-A kinase,[38] and blocks growth of aggressive cancers *in vivo* (mice bearing HPAF-II human pancreatic cancer xenografts) by inhibiting FGFR- and SRC-mediated signaling.[39]

We have also been interested in the development of antibiotic[40] and anticancer rhenium species.[41] In a recent study, we have reported the anti-proliferative efficacy of a series of *fac*-$[Re(I)(CO)_3]^+$ *N*-derivatized *N*-([2,2′-bipyridin]-6-ylmethyl)-species against colorectal carcinoma (CRC) and identified complex **1** (Chart 1) as a potent *in vivo* (zebrafish xenograft model of human CRC) anticancer, anti-angiogenic and anti-metastatic compound.[42] *In vivo*, compound **1** (1–3 μM concentration) is more potent than clinical drugs, such as cisplatin and sunitinib malate, and shows no signs of clinical toxicity (cardio-, hepato-, and myelotoxicity) at high concentrations (*i.e.*, 250 μM).

The identification of **1** amongst a series of related species, made us wonder if the presence and position of a reactive halomethyl substituent on the diimine ligand system of *fac*-$[Re(CO)_3]^+$ core may be a/the key molecular feature for the activity of **1** and for design of similar active and non-toxic anticancer agents. After all, **1** is of a relatively simple design, not dissimilar from other diimine rhenium compounds that, however, do not appear to be as promising as **1**, and the presence of the reactive halomethyl substituent is the unique feature of **1** in the series of compounds investigated. To this end, we have prepared a small library of 5- and 6-(halomethyl)-2,2′-bipyridine rhenium tricarbonyl complexes, and evaluated *in vivo* their anticancer activity against pancreatic and CRC tumors. Of the new species presented in this study, only one compound (5-(chloromethyl)-2,2′-bipyridine derivative) shows significant inhibition of pancreatic tumour growth in zebrafish-Panc-1 xenografts. The complex is also capable of inhibiting *in vivo* cancer cells dissemination, but it does not surpass the genuine potential of **1**. We describe our findings in the following sections.

2. Results and discussion

2.1. Chemistry

Ligands and rhenium complexes **1–10** were prepared according to the synthetic protocols illustrated in Scheme 1. The 2,2′-bipyridine derivatives were obtained *via* the well-established Pd-catalyzed Stille's C–C coupling reaction,[43] starting from commercially available reagents. The 5- and 6-(difluoromethyl)-2,2′-bipyridines ($\mathbf{L_5}$ and $\mathbf{L_{10}}$ in Scheme 1) were obtained in a single step in moderate yields of 17% and 38% respectively. Similarly [2,2′-bipyridin]-5- and 6-ylmethanol ($\mathbf{L_3}$ and $\mathbf{L_8}$) were obtained in good yield from the corresponding methyl [2,2′-bipyridine]-#-carboxylate following its reduction with $NaBH_4$. Ligands $\mathbf{L_3}$ and $\mathbf{L_8}$ were then converted to the 5- and 6-(halomethyl)-2,2′-bipyridines ($\mathbf{L_1}$, $\mathbf{L_2}$, $\mathbf{L_6}$ and $\mathbf{L_7}$) either by treatment with PBr_3 ($\mathbf{L_1}$ and $\mathbf{L_6}$) or thionyl chloride ($\mathbf{L_2}$ and $\mathbf{L_7}$). Finally, the rhenium complexes were obtained in high yield by treatment of *fac*-$[Re(CO)_5Br]$ with the corresponding 2,2′-bipyridine ligand in hot toluene[42] (Scheme 1).

^{1}H NMR spectra of complexes (ESI, Fig. S1–S9†) showed pure diamagnetic compounds, according to the symmetry given by the facial-arranged CO's and low-spin d^6 nature of the metal ion. IR spectroscopy analysis was in accordance with the typical tricarbonyl vibration pattern. Crystals suitable for X-ray diffraction analysis were obtained for seven of nine new species. Crystallographic details are given in ESI,† whereas Fig. 1 and 2 depict respectively the ORTEPs of the *meta*- and *ortho*-substituted derivative. Complexes **2**, **6**, **7**, **9** and **10** all crystallized in a monoclinic lattice and space groups *C*2/*c* (**2**), *P*21/*c* (**6**, **7** and **10**), Pc (**9**) respectively, whereas **3** and **5** were obtained in the triclinic space group $P\bar{1}$ and in the ortho-

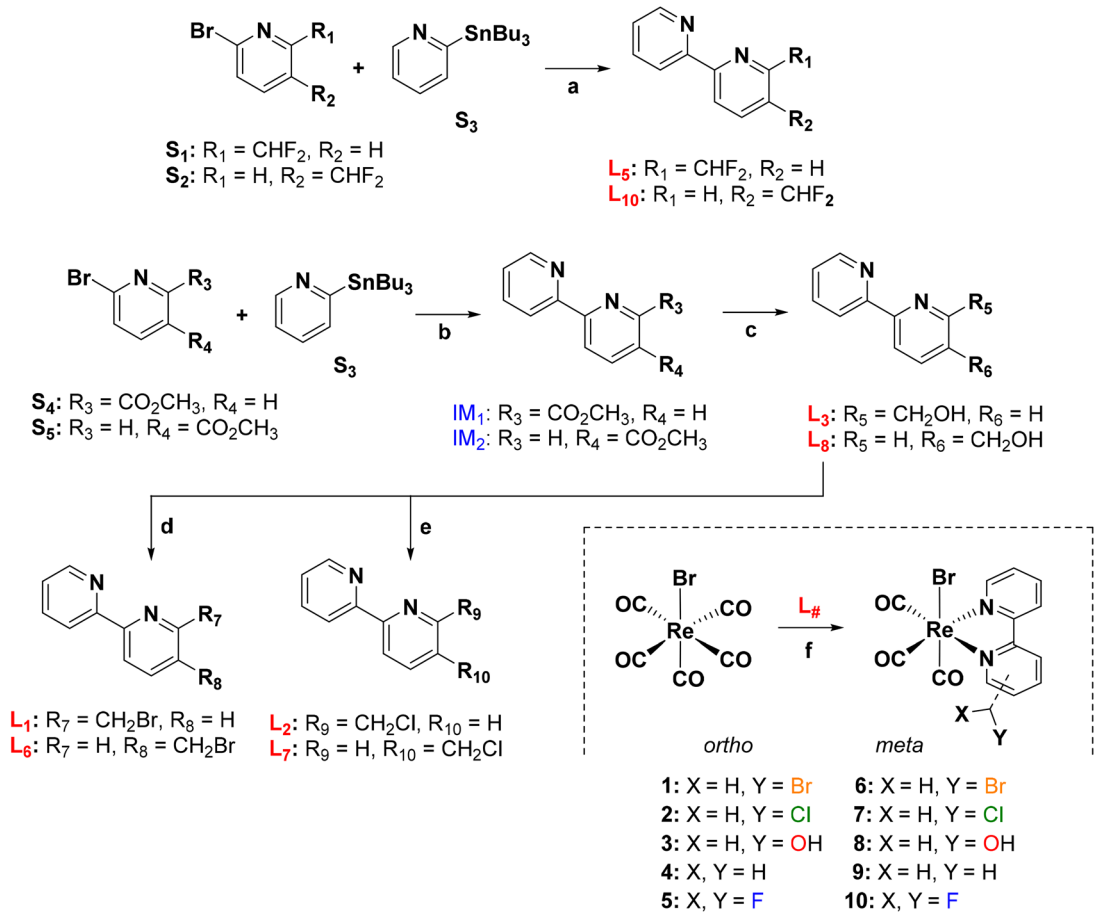

Scheme 1 Synthesis and chemical structures of bipyridine ligands ($L_{\#}$) and of Re complexes (bottom left). Conditions: (a) & (b) $Pd(PPh_3)_2(Cl)_2$, dry DMF, 130 °C, 10 h, under argon, 17–41%; (c) $NaBH_4$, ethanol, H_2O, 85 °C, 3 h, under argon, 76–79%; (d) PBr_3, dry DCM, rt, 10 h, under argon, 77–89%; (e) $SOCl_2$, $NaHCO_3$, 80 °C, 2 h, 80–83%, (f) and (a) toluene, 85–100 °C, 10–12 h, 68–96%.

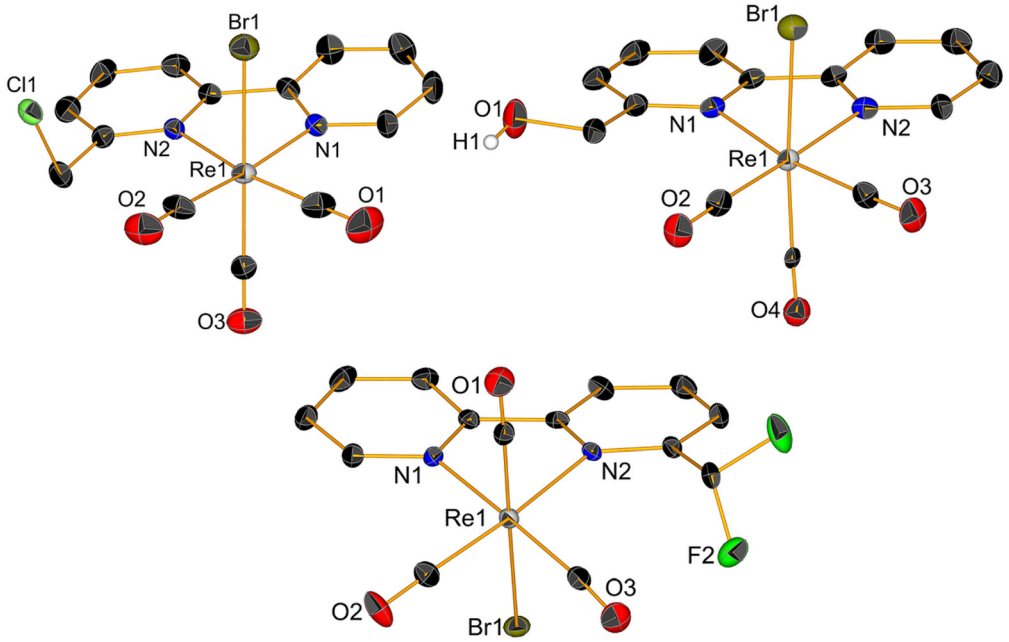

Fig. 1 Crystal structures of compounds **2**, **3** and **5**. Thermal ellipsoids are at 30% probability. Hydrogen atoms are omitted for clarity.

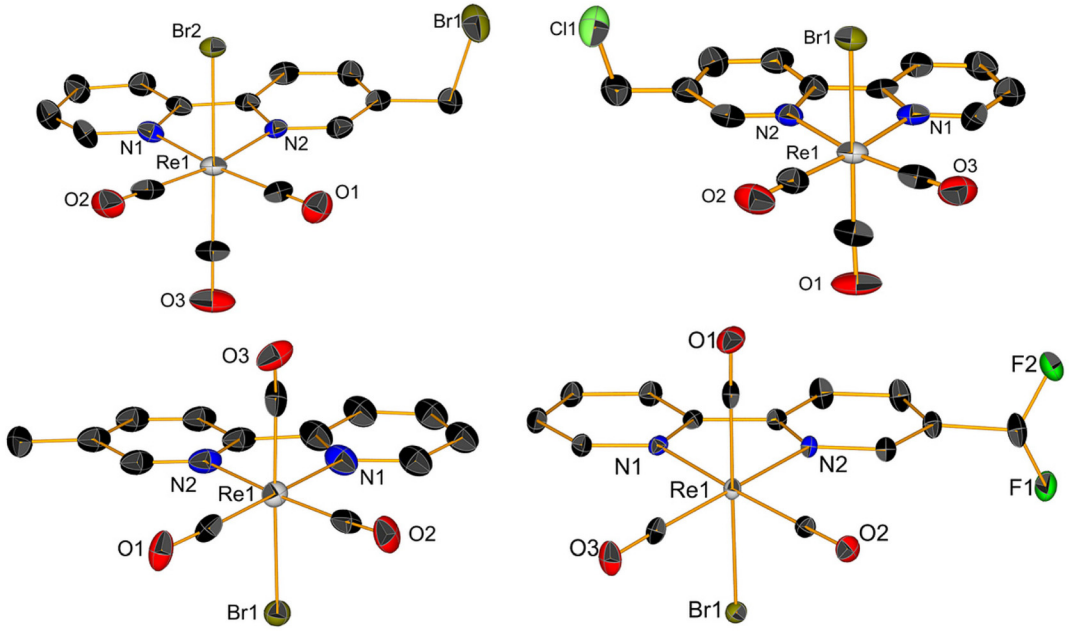

Fig. 2 Crystal structures of compounds **6**, **7**, **9** and **10**. Thermal ellipsoids are at 30% probability. Hydrogen atoms are omitted for clarity.

rhombic space group *Pca*21. All seven crystal structures of the complexes (Fig. 1 and 2) present a slightly distorted octahedral geometry around the central metal ion, but structural parameters are not significantly different from similar *fac*-[Re$(CO)_3]^+$ species (CCDC search).

Spectroscopically, **2–10** show the characteristic stretching bands expected for tricarbonyl complexes in the water-free region of their IR spectra. For all complexes, as predicted,[44] the pattern is very similar both in terms of frequency and in intensity of the stretching vibration. The UV-Vis spectra of the compounds display two main absorptions. All complexes show similar $\pi \rightarrow \pi^*$ intra-ligand transitions (LLCT) as sharp bands at 300 nm attributed to the diimine-ligand system. In addition, the spectra show a metal-to-ligand charge transfer transition (MLCT, responsible for the luminescent properties of the species) cantered at 370 nm.[45]

2.2. Relative lipophilicity of complexes

The activity of rhenium tricarbonyl anticancer drugs is often correlated to their lipophilicity.[10,46–51] The lipophilicity of the complexes is generally defined by octanol–water partition coefficient (log *P*, or K_{ow} value) referring to the ratio of the compound's concentration in the octanol phase to its concentration in the aqueous phase in the two-components system. Although previously we did not see a correlation between the lipophilicity and IC_{50} values of 6-(methyl-derivatized)-2,2′-bipyridine *fac*-$[Re(CO)_3]^+$ compounds, we decided to calculate and provide drug-likeness data of the complexes presented herein. We believe it is important to add such data in an era of computer-aided drug design of metal-based drug discovery. The drug-likeness properties of compounds **1–10** were calculated *via* the Molinspiration software. The results are given in

Table 1 Calculated molecular properties of investigated compounds for the assessment of drug-likeness

Complex	mi Log P^a	TPSA^b	M_W ^{c}	N_{atoms} ^{d}	N_{ON} ^{e}	N_{OHNH} ^{f}	N_{viol} ^{g}	N_{rotb} ^{h}	Vol.^{i}
1	3.78	61.08	602.28	22	5	0	1	4	297.04
2	3.65	61.08	557.83	22	5	0	1	4	292.69
3	2.41	81.31	539.38	22	6	1	1	4	287.17
4	3.06	61.08	523.38	21	5	0	1	3	278.91
5	3.61	61.08	559.36	23	5	0	1	4	289.04
6	3.88	61.08	602.28	22	5	0	1	4	297.04
7	3.75	61.08	557.83	22	5	0	1	4	292.69
8	2.51	81.31	539.38	22	6	1	1	4	287.17
9	3.62	61.08	523.38	21	5	0	1	3	278.91
10	3.71	61.08	559.36	23	5	0	1	4	289.04

[a] Octanolewater partition coefficient (log *P* value obtained using Molinspiration method). [b] Molecular polar surface area in Å^2. [c] Molecular weight. [d] Number of nonhydrogen atoms. [e] Number of hydrogen-bond acceptors (O and N atoms). [f] Number of hydrogen-bond donors (OH and NH groups). [g] Number of "Rule of five" violations. [h] Number of rotatable bonds. [i] Molecular volume in Å^3.

Table 1. Complexes, overall, show very similar lipophilicity with the chloro and bromo derivatives (*i.e.* compounds **1–2** and **6–7**) being the most lipophilic species and the hydroxo derivatives (**3** and **8**) the most hydrophilic. With the exception of their molecular weight, molecules rate well in the drug-likeness assessment (Table 1).

2.3. *In vitro* anticancer activity evaluation

The antiproliferative effect of compounds **2–10** was evaluated on a panel of four cancer cell lines (2 colorectal and 2 pancreatic) and compared to the previously reported activity of **1**. In addition, the toxicity of all new complexes was assessed on a normal cell line (MRC-5) in order to determine the selectivity index (Si) of the molecules. Table 2 presents the results of our analysis. As evident from the data, the potentially alkylating (*i.e.* "*reactive*") chloro- and bromomethyl complexes **2**, **6** and **7** showed higher antiproliferative activity, as compared to the *unreactive* complexes. Of these latter species, only **4** (*i.e.* the 6-methyl-2,2′-bipyridine complex) revealed comparable activity to **2**, **6** and **7**. As it is the case for **1**, the compounds are particularly effective against the colorectal HCT-116 cell line, with IC_{50} values ranging from *ca.* 5 to 10 μM. We consider this result of

Table 2 *In vitro* cytotoxicity (IC_{50}, μM) and *in vivo* toxicity (LC_{50}, μM) of complexes **1–10**. The selectivity index (Si)/therapeutic index (Ti) are shown in brackets

	HT-29	HCT-116	MiaPaCa-2	Panc-1	MRC-5	Zebrafish[a]
Cells/comp.	IC_{50} (Si/Ti)[b]					LC_{50}
1	nd	**5.0 (6.8/48.9)**	**10.7 (3.2/22.8)**	nd	34	244.4
2	14.9	**10.3**	14.6	13.3	12	68.9
3	49.5	27.7	20.3	20.1	>50	nd
4	38.7	**9.5** (2.4/**5.1**)	39.6	**10.1 (2.3/4.9)**	23	48.6
5	25	21.8	19.3	16.5	25.3	nd
6	11.6	**7.5** (1.6/**6.5**)	12	16.7	12.3	49.1
7	16.9	**4.9 (3.2/7)**	**9.2** (1.7/3.7)	**11** (1.4/**3.1**)	15.5	34.2
8	302.8	31.8	33.1	23.1	49.3	nd
9	173.2	22.1	21.8	16.4	>50	nd
10	32.9	21.5	21	20.1	>50	nd

nd = not determined. [a] The LC_{50} values have been determined in the zebrafish model only for the compounds with the IC_{50} values ≤11 μM. [b] Selectivity index (Si) is determined as the ratio between IC_{50} values on the normal and tumour cell lines; therapeutic index (Ti) is determined as the ratio between corresponding LC_{50} and IC_{50} values. The most potent compounds showing the $IC_{50} \leq 11$ μM and/or Si ≥ 3 and Ti ≥ 4 are bolded.

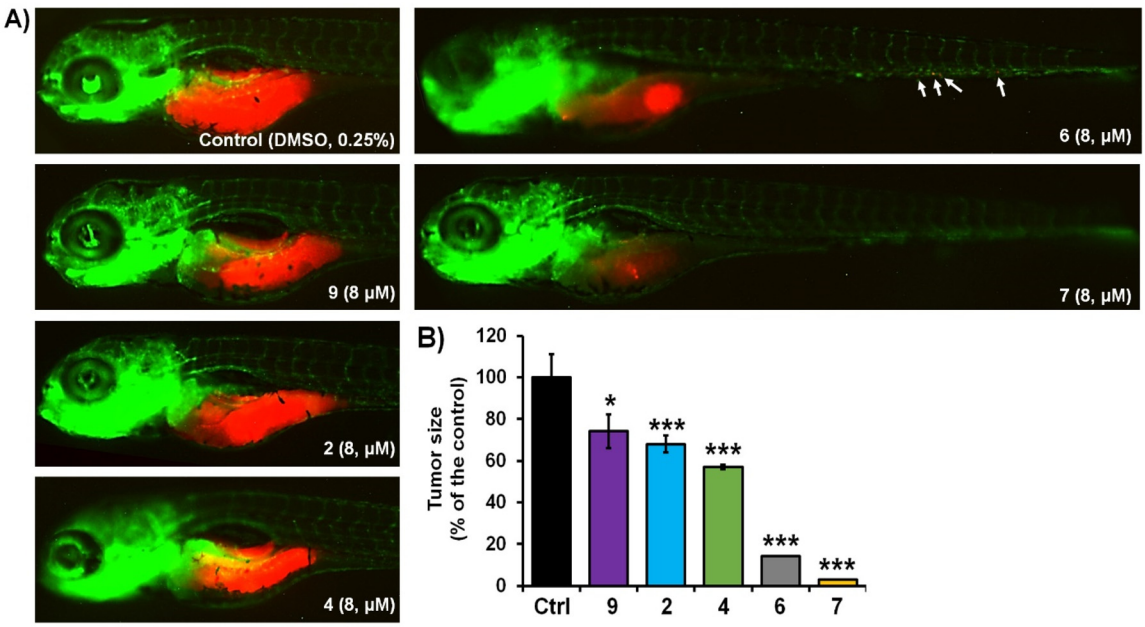

Fig. 3 Anticancer activity of selected complexes against human Panc-1 cells in zebrafish xenografts. *Tg*(*fli1*:EGFP) xenografts (*n* = 20) were exposed to complexes at 8 μM doses, and then analysed after 3-days treatments for tumour progression and metastasis. Representative fluorescent microscopy images are shown (A); white solid arrows indicate disseminated cells. Only applied treatments of complexes **6** and **7** markedly reduced the tumour, growth compared to those in the control group (B). Data are normalized in relation to the control group (B). **P* < 0.05; ***P* < 0.01; ****P* < 0.001.

particular relevance since HCT-116 is a CRC cell line that rapidly acquires resistance to clinical anticancer drugs, including cisplatin, oxaliplatin, docetaxel, 5-FU, and others.[52–55] As we have previously pointed out,[42] it is possible that unique characteristics of HCT-116 cells, including mutation in the KRAS proto-oncogene, exhibitions of wild-type p53 expression, stem cell-like properties, low differentiation level, fast division as well as epithelial morphology,[55–57] could all be factors contributing to their higher sensitivity of tumor line this class of rhenium tricarbonyl complexes. Unlike **1**, however, the new compounds show in general a lower Si (Table 2) towards cancer cells, being only *ca.* twice as active when compared to the IC_{50} value against healthy MRC-5 cells. Only complex **7** showed moderately good selectivity towards HCT-116 with an Si of 3.1. Nevertheless, we decided to further investigate *in vivo* selected compounds with acceptable Si (here defined as Si > 1).

2.4. *In vivo* anticancer activity in the zebrafish xenograft models

The activity of complexes **2**, **4**, **6**, **7** and **9** was finally investigated *in vivo* against human pancreatic and colorectal carcinoma tumours using the zebrafish-Panc-1 and -HCT-116 xenograft models. Zebrafish xenografts are an established platform for translational research to human cancers, allowing the study of key hallmarks of cancer biology, such as tumour cells proliferation, dissemination, metastasis and angiogenesis.[56,58,59] Accordingly, in two separate experiments, Panc-1 and HCT-116 cells were fluorescently labelled and injected into the yolk of *Tg(fli1*:EGFP) and *Tg(-2.8fabp10a*:EGFP) embryos, respectively (Fig. 3 and 4). At 3 days post injection (dpi), xenografts were processed for fluorescence microscopy in order to evaluate the effects of applied complexes on the tumour mass development and cancer cells dissemination and metastasis.

Our results of zebrafish-Panc-1 xenografts (Fig. 3) show that only treatments with **6** and **7** significantly inhibited pancreatic tumour growth *in vivo* ($P < 0.001$). Compound **7** was also effective in inhibiting cancer cells dissemination ($P < 0.001$). Both complexes were noticeably effective at an 8 μM concentration, lower than their respective *in vitro* IC_{50} values (Table 2). Comparison of tumour growth to untreated Panc-1 xenografts at 3 dpi (120 hpf) indicated that **6** and **7** reduced tumour mass in the treated xenografts by 86.0 ± 1.0% and 97.5 ± 0.5%, respectively ($P < 0.0001$, for both compounds). Compound **7** was also the most effective complex of the series

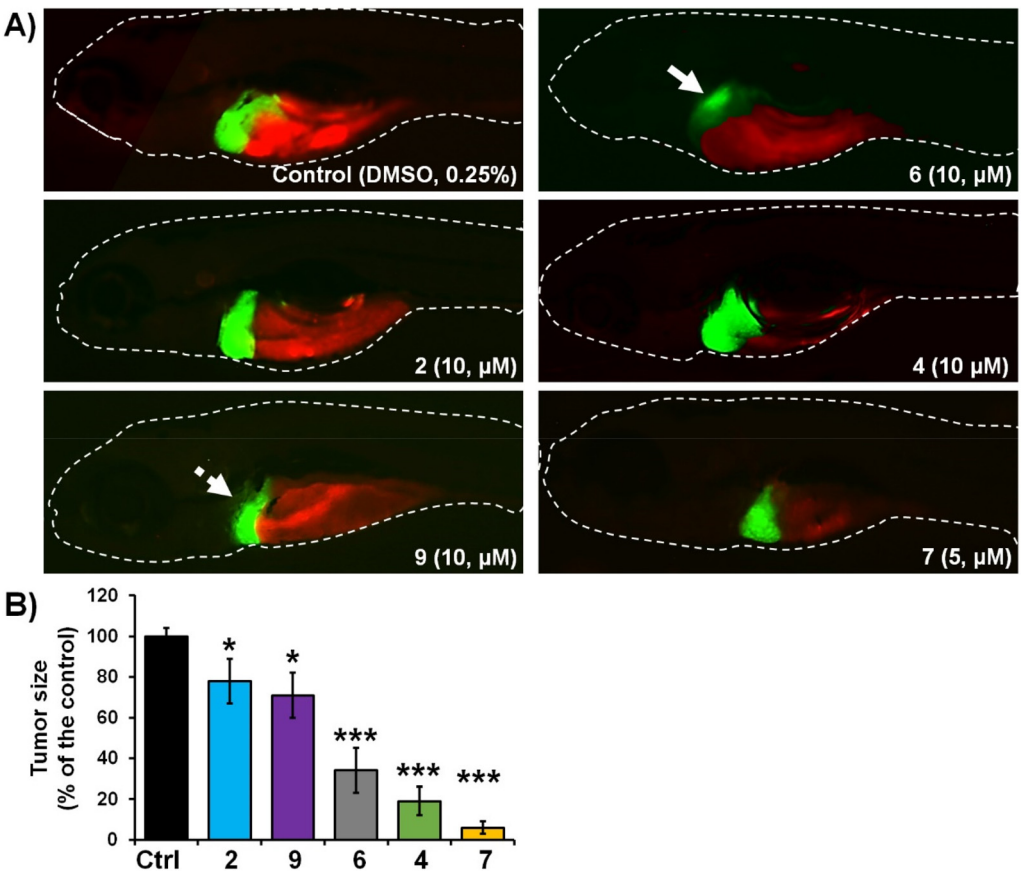

Fig. 4 Anticancer activity of selected complexes against highly metastatic human HCT-116 cells in zebrafish xenografts. *Tg(-2.8fabp10a*:EGFP) xenografts (n = 20) were exposed to complexes at 10 μM doses, and then analysed after 3-day treatments for tumour progression and metastasis. Representative fluorescent microscopy images are shown (A); white solid arrow indicates treatment-affected liver (hepatotoxicity). Only applied treatments of complexes **4** and **7** markedly reduced the tumour growth, compared to those in the control group (B). Data are normalized in relation to the control group (B and C). *$P < 0.05$; **$P < 0.01$; ***$P < 0.001$.

in inhibiting colorectal tumour growth in zebrafish-HCT-116 xenografts (Fig. 4). However, significant cancer growth inhibition was archived at 2× *in vitro* IC_{50} value of the compound (*i.e.* at 10 μM). In zebrafish-HCT-116 xenografts, **6** showed much lower efficacy than in the pancreatic xenograft model (66.4 ± 11.1% *vs.* 86.1 ± 4.2%, $P < 0.0001$). Finally, in the colorectal carcinoma model, compound **4** showed good inhibition of tumour growth (80.9 ± 7.3%, $P < 0.0001$).

3. Conclusion

We have reported the synthesis, characterization, and *in vivo* evaluation of the anticancer activity of a series of 5- and 6-(halomethyl)-2,2′-bipyridine rhenium tricarbonyl complexes. On the basis of the initial identification of compound **1**,[42] the study was initiated in order to understand if the presence and position of a reactive halomethyl substituent on the diimine ligand system of *fac*-$[Re(CO)_3]^+$ species may be a key structural or molecular feature for the design of active and non-toxic anticancer agents. Overall, our study revealed that, within the series of methyl-substituted diimine complexes, only compounds potentially able of ligand-based alkylating reactions (*i.e.* chloro- and bromomethyl complexes **2**, **6** and **7**) showed significant antiproliferative activity (as compared to the *unreactive* complexes, which are generally inactive). Of the new species presented in this study, compound **7** showed significant inhibition of pancreatic tumour growth *in vivo* in zebrafish-Panc-1 xenografts. The complex is noticeably effective at 8 μM concentration, lower than its *in vitro* IC_{50} values, and it is also effective in inhibiting cancer cells dissemination, but it does not surpass the genuine potential of **1**.

4. Experimental protocols

4.1. Materials and methods

All chemical reagents were purchased as reagent or analytical grade from commercial suppliers (Sigma-Aldrich, Alfa Aesar, TCI, Fluorochem) and used without further purification. Solvents were either used as received or dried over molecular sieves prior to use. ^1H and ^{13}C NMR spectra were recorded on a Bruker Avance III 400 MHz using residual solvent peaks as internal references. The following abbreviations are used: singlet (s), doublet (d), doublet of doublets (dd), triplet (t), doublet of triplets (td), quintuplet (quint), sextuplet (sext), and multiplet (m). HPLC analysis was performed on a Merck-Hitachi L7000. The analytical separations were conducted on a Machereye Nagel Nucleodur PolarTec column (5 μm particle size, 110 Å pore size, 250/3). The preparative separations were conducted on a Machereye Nagel Nucleodur C18 HTec column (5 μm particle size, 110 Å pore size, 250/21). The flow rate was set to 0.5 mL min^{-1} for analytical separations and 5 mL min^{-1} for the preparative ones. Eluting solvents and gradient are as previously described.[60] The eluting bands were detected at 250 nm. Analytical thin-layer chromatography (TLC) was performed on commercial silica plates (Merck 60-F 254, 0.25 mm thickness); compounds were visualized by UV light (254 nm and 366 nm). Preparative flash chromatography was performed with Merck silica gel (Si 60, 63–200 mesh). IR spectra were recorded on a PerkinElmer Spectrum 100 FT-IR spectrometer. The UV-Vis spectra were recorded on a Jasco V-730 and the emission on a spectrofluorometer FS5 (Edinburgh Instruments Ltd). Single crystal diffraction data collection was performed on a Stoe IPDS2 diffractometer (CuKα1 (λ = 1.5406 Å)) equipped with a cryostat from Oxford Cryosystems. The structures were solved with the ShelXT structure solution program using Intrinsic Phasing and refined with the ShelXL refinement package using Least Squares minimization.[61,62] All crystal structures are deposited at the Cambridge Crystallographic Data Centre. CCDC numbers 2090791–2090797 contain the supplementary crystallographic data for this paper.†

4.2. Synthesis and characterization of ligands and complexes

4.2.1. General procedure for the preparation of ligands

*Preparation of 6-(difluoromethyl)-2,2′-bipyridine (**L_5**) and 5-(difluoromethyl)-2,2′-bipyridine (**L_{10}**).* 2-Bromo-6-(difluoromethyl)pyridine (**S_1**, or 2-bromo-5-(difluoromethyl)pyridine **S_2**, for **L_5** and **L_{10}** respectively, 1.0 equiv.) was added to a suspension of 2-(tributylstannyl)pyridine (**S_3**, 1.2 equiv.) in dry DMF. $Pd(PPh_3)_2(Cl)_2$ (cat.) was added under inert conditions, and then the reaction mixture was heated to 130 °C and stirred overnight. After completion of the reaction, the mixture was cooled to room temperature, and filtered over Celite. The residue was washed with DMF until the filtrate was colourless. The filtrate was evaporated and residue was dissolved in water. The solution was extracted 3 times with DCM, washed with brine, the combined organic phase was dried with $MgSO_4$ and then solvent was evaporated. The crude product was purified by flash column chromatography using DCM/MeOH 98 : 2 (v : v) to give a dark solid. This was dissolved in a small amount of diethyl ether followed by the addition of pentane. The solution was stirred overnight, then filtered and the residue washed with cold pentane. In order to increase the yield, the filtrate was evaporated and then precipitated again in pentane. The combined products were dried to give the desired compounds. Yields for **L_5** and **L_{10}** were 17% and 38% respectively. **L_5**: ^1H NMR (400 MHz, $CDCl_3$) δ ppm 6.58–6.88 (m, 1 H), 7.35 (ddd, J = 7.46, 4.77, 1.22 Hz, 1 H), 7.67 (d, J = 7.70 Hz, 1 H), 7.85 (td, J = 7.76, 1.83 Hz, 1 H), 7.98 (t, J = 7.83 Hz, 1 H), 8.47 (dt, J = 7.95, 1.04 Hz, 1 H), 8.55 (dd, J = 7.95, 0.98 Hz, 1 H), 8.69–8.73 (m, 1 H). **L_{10}**: ^1H NMR (400 MHz, $CDCl_3$) δ ppm 6.62–6.94 (m, 1 H), 7.36 (ddd, J = 7.46, 4.77, 1.10 Hz, 1 H), 7.85 (td, J = 7.73, 1.77 Hz, 1 H), 7.97 (dt, J = 8.25, 0.95 Hz, 1 H), 8.45 (d, J = 7.95 Hz, 1 H), 8.53 (d, J = 8.19 Hz, 1 H), 8.71 (dd, J = 4.71, 0.67 Hz, 1 H), 8.81 (d, J = 0.73 Hz, 1 H).

*Preparation of methyl [2,2′-bipyridine]-6-carboxylate (**IM_1**) and methyl [2,2′-bipyridine]-5-carboxylate (**IM_2**).* The same procedure described above for the preparation of **L_5** and **L_{10}** was used starting with methyl 6-bromopicolinate (**S_4**, or methyl 6-bromonicotinate **S_5**, for **IM_1** and **IM_2** respectively, 1.0 equiv.) and S_3

(1.2 equiv.). Yields for IM_1 and IM_2 were 47% and 41% respectively. Analytical data are in agreement with data reported in literature for IM1[63,64] and IM2.[65]

*Preparation of [2,2'-bipyridin]-6-ylmethanol (**L₃**) and [2,2'-bipyridin]-5-ylmethanol (**L₈**).* Under argon, IM_1 (or IM_2, for L_3 and L_8 respectively, 1.0 equiv.) was dissolved in ethanol followed by the portion wise addition of $NaBH_4$ (3.0 equiv.). At the end of the addition, the reaction mixture was heated to 85 °C and stirred for 3 h. After completion of the reaction, the solution was cooled down to room temperature and quenched by the addition of H_2O. The residual ethanol was evaporated, and the solution acidified by the addition of sulphuric acid and then washed 3 times with DCM. The aqueous phase was basified with NaOH 30% and extracted 3 times with DCM. The combined organic phase was then dried with $MgSO_4$. Evaporation of the solvent gave the pure products. Yields for L_3 and L_8 were 79% and 76% respectively. Analytical data are in agreement with data reported in literature for L_3 [66] and L_8.[67]

*Preparation of 6-(bromomethyl)-2,2'-bipyridine (**L₁**) and 5-(bromomethyl)-2,2'-bipyridine (**L₆**).* L_3 (or L_8, for L_1 and L_6 respectively, 1.0 equiv.) was dissolved in dry DCM under inert conditions while being cooled in an ice bath, followed by a slow addition of PBr_3 (3.0 equiv.). The ice bath was then removed, and the reaction mixture was stirred overnight at room temperature. After completion of the reaction, the solution was cooled again in an ice bath, and the reaction was quenched by the slow addition of cold water. Residual DCM was evaporated, and the residue was basified by the addition of NaOH 30%. For L_1, the solution was filtered, and the residue was washed with cold water. For L_6, the mixture was extracted 3 times with DCM, washed with water and dried with $MgSO_4$. The residual solvent was evaporated to give the desired product. Yields for L_1 and L_6 were 77% and 89% respectively. Analytical data are in agreement with data reported in literature for L_1 and L_6.[68]

*Preparation of 6-(chloromethyl)-2,2'-bipyridine (**L₂**) and 5-(chloromethyl)-2,2'-bipyridine (**L₇**).* L_3 (or L_8, for L_2 and L_7 respectively, 1.0 equiv.) was placed in a beaker and the solid was cooled in an ice bath before the dropwise addition of thionyl chloride (17.0 equiv.). Then the reaction mixture was heated to 80 °C and stirred for 2 h. After completion of the reaction, the solution was cooled to room temperature and excess thionyl chloride was evaporated. The orange residue was then gently added to a saturated $NaHCO_3$ solution. The mixture was extracted 3 times with ethyl acetate, washed with brine, and dried with $MgSO_4$. The solvent was evaporated and the residue was purified by normal phase column chromatography using pentane/ethyl acetate 5 : 1 (v : v) to give the desired product. Yields for L_2 and L_7 were 83% and 80% respectively. Analytical data are in agreement with data reported in literature for L_7 [69] and L_2.[70]

4.2.2. General procedure for the preparation of *fac*-[Re(CO)₃(L#)Br] complexes 1–10. Bromopentacarbonylrhenium(I) (1.0 equiv.) was dissolved in hot toluene (60 °C) under argon. The diimine ligand (1.0 equiv.) was added, and the solution was refluxed overnight at 85–95 °C. The reaction mixture was cooled to room temperature, and then placed in the fridge for 1 h. The formed precipitate was filtered off, washed with cold toluene, and dried *in vacuo*. Generally, no further purification was necessary to give the pure products described below.

*fac-[Re(CO)₃(**L₂**)Br] (**2**).* Yellow powder, yield 96%. ESI-MS analysis (positive mode) m/z = 474.9 $[M - Br]^+$ measured; calculated for $[C_{14}H_9ClN_2O_3Re]^+$ 475.0. IR (solid, νCO cm^{-1}): 2015.43, 1882.86. UV-Vis (CH_3CN, nm): 301, 372. ^{1}H NMR (400 MHz, acetonitrile-d3) δ ppm 5.11–5.23 (m, 2 H) 7.65 (ddd, J = 7.64, 5.56, 1.10 Hz, 1 H) 7.89–8.01 (m, 1 H) 8.14–8.28 (m, 2 H) 8.35–8.49 (m, 2 H) 9.06–9.15 (m, 1 H). ^{13}C NMR (126 MHz, acetonitrile-d_3) δ ppm 48.64–51.40 (m, 1 C) 123.48–126.23 (m, 3 C) 126.65–128.85 (m, 2 C) 139.05–142.77 (m, 3 C) 153.49 (d, J = 4.54 Hz, 2 C). Crystals suitable for X-ray diffraction were obtained from layering of hexane on DCM.

*fac-[Re(CO)₃(**L₃**)Br] (**3**).* Yellow powder, yield 96%. ESI-MS analysis (positive mode) m/z = 456.9 $[M - Br]^+$ measured; calculated for $[C_{14}H_{10}N_2O_4Re]^+$ 457.0. IR (solid, νCO cm^{-1}): 2015.70, 1919.28, 1889.42. UV-Vis (CH_3CN, nm): 299.5, 367.5. ^{1}H NMR (400 MHz, DMSO-d6) δ ppm 4.81–4.96 (m, 2 H) 6.20 (br. s., 1 H) 7.72–7.78 (m, 1 H) 8.00 (d, J = 7.93 Hz, 1 H) 8.28–8.37 (m, 2 H) 8.65 (d, J = 7.93 Hz, 1 H) 8.76 (d, J = 8.24 Hz, 1 H) 9.07 (d, J = 5.34 Hz, 1 H). ^{13}C NMR (126 MHz, DMSO-d_6) δ ppm 67.53 (s, 1 C) 122.55 (s, 1 C) 123.87 (s, 1 C) 124.55 (s, 1 C) 127.74 (s, 1 C) 140.49 (d, J = 14.53 Hz, 1 C) 152.77 (s, 1 C) 155.53 (s, 1 C) 156.14 (s, 1 C) 164.80 (s, 1 C) 188.44 (s, 1 C) 197.05 (s, 1 C). Crystals suitable for X-ray diffraction were obtained from layering of hexane on DCM.

*fac-[Re(CO)₃(**L₄**)Br] (**4**).* Yellow powder, yield 91%. ESI-MS analysis (positive mode) m/z = 440.9 $[M - Br]^+$ measured; calculated for $[C_{14}H_{10}N_2O_3Re]^+$ 441.0. IR (solid, νCO cm^{-1}): 2017.70, 1896.71. UV-Vis (CH_3CN, nm): 299, 369. ^{1}H NMR (400 MHz, acetonitrile-d3) δ ppm 3.01 (s, 3 H) 7.57–7.69 (m, 2 H) 8.04 (t, J = 7.89 Hz, 1 H) 8.12–8.20 (m, 1 H) 8.26 (d, J = 7.95 Hz, 1 H) 8.35–8.41 (m, 1 H) 9.04–9.12 (m, 1 H). ^{13}C NMR (126 MHz, acetonitrile-d3) d ppm 17.67 (s, 1 C) 123.73 (d, J = 17.26 Hz, 1 C) 127.29 (s, 1 C) 138.26 (s, 1 C) 139.20–141.08 (m, 2 C) 151.49–153.45 (m, 2 C) 155.21 (s, 1 C).

*fac-[Re(CO)₃(**L₅**)Br] (**5**).* Yellow powder, yield 95%. ESI-MS analysis (positive mode) m/z = 476.9 $[M - Br]^+$ measured; calculated for $[C_{14}H_8F_2N_2O_3Re]^+$ 477.0. IR (solid, νCO cm^{-1}): 2017.49 1889.73. UV-Vis (CH_3CN, nm): 296, 377. ^{1}H NMR (400 MHz, DMSO-d6) δ ppm 7.17–7.42 (m, 1 H) 7.80 (t, J = 6.41 Hz, 1 H) 7.91 (d, J = 5.65 Hz, 1 H) 8.35 (t, J = 7.86 Hz, 1 H) 8.91 (d, J = 8.09 Hz, 1 H) 8.94 (s, 1 H) 9.07 (s, 1 H) 9.20 (d, J = 5.65 Hz, 1 H). ^{13}C NMR (126 MHz, DMSO-d_6) d ppm 110.58 (s, 1 C) 112.49 (s, 1 C) 114.40 (s, 1 C) 120.43–121.34 (m, 1 C) 123.03–124.59 (m, 1 C) 124.84 (s, 1 C) 128.18 (s, 1 C) 140.19 (s, 1 C) 143.85–145.74 (m, 1 C) 153.07 (s, 1 C) 153.67–154.97 (m, 1 C) 156.26 (s, 1 C) 188.91 (s, 1 C) 196.99 (d, J = 16.35 Hz, 1 C). Crystals suitable for X-ray diffraction were obtained from layering of hexane on DCM.

*fac-[Re(CO)₃(**L₆**)Br] (**6**).* Yellow powder, yield 68%. ESI-MS analysis (positive mode) m/z = 519.1 $[M - Br]^+$ measured; calculated for $[C_{14}H_9BrN_2O_3Re]^+$ 518.9. IR (solid, νCO cm^{-1}): 2016.66, 1882.55. UV-Vis (CH_3CN, nm): 298, 384. ^{1}H NMR (400 MHz, DMSO-d6) δ ppm 4.96 (s, 2 H) 7.71–7.80 (m, 1 H)

8.33 (t, J = 7.86 Hz, 1 H) 8.40 (d, J = 8.39 Hz, 1 H) 8.76 (t, J = 8.70 Hz, 2 H) 9.04 (d, J = 5.34 Hz, 1 H) 9.12 (s, 1 H). ^{13}C NMR (126 MHz, DMSO-d6) δ ppm 14.04 (s, 2 C) 22.33 (s, 1 C) 27.04 (s, 1 C) 34.12 (s, 1 C) 54.55 (s, 1 C) 121.76–124.24 (m, 1 C) 127.25 (s, 1 C) 136.74–140.99 (m, 2 C) 151.71–156.38 (m, 1 C). Crystals suitable for X-ray diffraction were obtained from layering of pentane on chloroform.

*fac-[Re(CO)$_3$(**L$_7$**)Br] (**7**).* Yellow powder, yield 81%. ESI-MS analysis (positive mode) m/z = 474.9 $[M - Br]^+$ measured; calculated for $[C_{14}H_9ClN_2O_3Re]^+$ 475.0. IR (solid, νCO cm^{-1}): 2017.48, 1882.97. UV-Vis (CH_3CN, nm): 296, 276. ^{1}H NMR (400 MHz, DMSO-d6) δ ppm 5.05 (s, 2 H) 7.77 (br. s., 1 H) 8.34 (s, 1 H) 8.41 (d, J = 7.17 Hz, 1 H) 8.79 (dd, J = 15.87, 8.24 Hz, 2 H) 9.05 (d, J = 5.49 Hz, 1 H) 9.12 (s, 1 H). ^{13}C NMR (126 MHz, DMSO-d6) δ ppm 41.53 (s, 1 C) 123.27–125.47 (m, 2 C) 127.97 (s, 1 C) 137.83 (s, 1 C) 139.26–141.18 (m, 2 C) 150.56–154.00 (m, 2 C) 154.00–155.79 (m, 2 C) 189.29 (s, 1 C) 195.62–197.55 (m, 2 C). Crystals suitable for X-ray diffraction were obtained from layering of hexane on DCM.

*fac-[Re(CO)$_3$(**L$_8$**)Br] (**8**).* Yellow powder, yield 68%. ESI-MS analysis (positive mode) m/z = 456.9 $[M - Br]^+$ measured; calculated for $[C_{14}H_{10}N_2O_4Re]^+$ 457.0. IR (solid, νCO cm^{-1}): 2016.90, 1869.77. UV-Vis (CH_3CN, nm): 294, 371. ^{1}H NMR (400 MHz, DMSO-d6) δ ppm 4.74 (d, J = 5.65 Hz, 2 H) 5.73 (t, J = 5.72 Hz, 1 H) 7.71–7.77 (m, 1 H) 8.22 (d, J = 8.24 Hz, 1 H) 8.32 (t, J = 7.86 Hz, 1 H) 8.73 (d, J = 8.39 Hz, 2 H) 8.96 (s, 1 H) 9.02 (d, J = 5.49 Hz, 1 H). ^{13}C NMR (126 MHz, DMSO-d6) δ ppm 59.69 (s, 1 C) 122.58–124.92 (m, 2 C) 127.58 (s, 1 C) 137.89 (s, 1 C) 140.18 (s, 1 C) 142.51 (s, 1 C) 150.48 (s, 1 C) 152.35–154.28 (m, 2 C) 155.16 (s, 1 C) 189.45 (s, 1 C) 197.38 (s, 1 C) 201.66 (s, 1 C).

*fac-[Re(CO)$_3$(**L$_9$**)Br] (**9**).* Yellow powder, yield 74%. ESI-MS analysis (positive mode) m/z = 440.9 $[M - Br]^+$ measured; calculated for $[C_{14}H_{10}N_2O_3Re]^+$ 441.0. IR (solid, νCO cm^{-1}): 2017.70, 1896.71. UV-Vis (CH_3CN, nm): 295, 368. ^{1}H NMR (400 MHz, DMSO-d6) δ ppm 2.50 (s, 3 H) 7.68–7.76 (m, 1 H) 8.16 (d, J = 8.39 Hz, 1 H) 8.30 (t, J = 7.86 Hz, 1 H) 8.62–8.73 (m, 2 H) 8.86 (s, 1 H) 9.01 (d, J = 5.34 Hz, 1 H). ^{13}C NMR (126 MHz, DMSO-d_6) d ppm 17.67 (s, 1 C) 123.79 (s, 2 C) 127.29 (s, 1 C) 138.26 (s, 1 C) 140.00 (s, 1 C) 140.51 (s, 1 C) 151.94–153.15 (m, 2 C) 155.21 (s, 1 C) 189.41 (s, 1 C) 197.12 (s, 2 C) 206.33 (s, 1 C). Crystals suitable for X-ray diffraction were obtained from layering of pentane on DCM.

*fac-[Re(CO)$_3$(**L$_{10}$**)Br] (**10**).* Yellow powder, yield 71%. ESI-MS analysis (positive mode) m/z = 476.9 $[M - Br]^+$ measured; calculated for $[C_{14}H_8F_2N_2O_3Re]^+$ 477.0. IR (solid, νCO cm^{-1}): 2020.67, 1887.81. UV-Vis (CH_3CN, nm): 295, 378. ^{1}H NMR (400 MHz, DMSO-d_6) δ ppm 7.26–7.51 (m, 1 H) 7.82 (t, J = 6.56 Hz, 1 H) 8.37 (t, J = 7.86 Hz, 1 H) 8.57 (d, J = 8.55 Hz, 1 H) 8.82–8.94 (m, 2 H) 9.08 (d, J = 5.34 Hz, 1 H) 9.19 (s, 1 H). ^{13}C NMR (126 MHz, DMSO-d6) d ppm 20.89 (s, 1 C) 110.28 (s, 1 C) 112.17 (s, 1 C) 114.07 (s, 1 C) 122.35–126.48 (m, 2 C) 127.17–129.93 (m, 2 C) 140.24 (s, 1 C) 150.39 (t, J = 7.72 Hz, 1 C) 153.17 (s, 2 C) 188.90 (s, 1 C) 196.87 (d, J = 18.17 Hz, 1 C). Crystals suitable for X-ray diffraction were obtained from layering of hexane on DCM.

4.3. Cytotoxicity evaluation

Antiproliferative activity of the compounds was tested in a panel against tumour cells lines HCT-116 (colorectal carcinoma cells), HT-29 (colorectal adenocarcinoma cells) Mia PaCa-2 (pancreatic carcinoma cells) and Panc-1 (epithelial pancreatic carcinoma cells), as well as on normal human lung fibroblasts (MRC-5), all from ATCC collection. Compounds were freshly dissolved in DMSO and used for the bioactivity assessments. Cytotoxicity in terms of antiproliferative effects was tested by the standard 3-(4,5-dimethylthiazol-2-yl)-2,5-diphenyltetrazolium bromide (MTT) assay.[71] The assay was carried out as previously described.[42]

4.4. *In vivo* toxicity assessment

Toxicity evaluation of the complexes was carried in the zebrafish (Danio rerio) model according to the general rules of the OECD Guidelines for the Testing of Chemicals (OECD, 2013, Test No. 236).[72] All experiments involving zebrafish were performed in compliance with the European directive 2010/63/EU and the ethical guidelines of the Guide for Care and Use of Laboratory Animals of the Institute of Molecular Genetics and Genetic Engineering, University of Belgrade. Wild type (AB) zebrafish were kindly provided by Dr Ana Cvejić (Wellcome Trust Sanger Institute, Cambridge, UK). Experiments were performed as previously reported.[42]

4.5. Anticancer activity evaluation in human CRC-zebrafish xenografts

Cancer cells were cultured in RPMI-1640 supplemented with 10% FBS, 100 μg mL^{-1} streptomycin and 100 U mL^{-1} penicillin, and grown as a monolayer in humidified atmosphere of 95% air and 5% CO_2 at 37 °C. Prior to microinjection, the cells were washed once with PBS and trypsinized (0.25% trypsin/0.53 mM EDTA) to obtain a single cell suspension. After centrifugation at 1200 rpm for 5 min, the cells were resuspended in serum-free RPMI medium and labelled with 2 μM CellTracker™ RedCMTPX (Thermofisher Scientific) according to the manufacturer's instructions.

4.6. Zebrafish xenografts injection and treatment

The zebrafish xenografts with human HCT-116 cells were established according to the previously described procedure.[73] Before the microinjections, Tg(fli1:EGFP) and *Tg(-2.8fabp10a*:EGFP) embryos were kept at 28 °C and manually dechorionated few hours before the injection. At 48 hpf, 5 nL of cells suspension containing 150 labelled cells was microinjected into the yolk of anesthetized embryos by a pneumatic picopump (PV820, World Precision Instruments, USA). Exact number of cells was confirmed by dispensing the injected volume onto a microscope slide and by visual counting. After injection, embryos were incubated to recover for at least one hour at 28 °C, dead embryos were removed, and alive embryos were transferred into 24-well plates containing 1 mL of embryo water and 10 embryos per well. The injected xenografts were treated with different doses of complex **1** and **4** (1/2, 1/4 and 1/

8 of IC_{50} values), and maintained at 33 °C by 120 hpf. DMSO (0.25%) was used as a negative control. The survival and development of the xenografted embryos was recorded every day until the end of experiment. At 3 days post injection (dpi), anesthetized xenografts were processed by fluorescent microscopy. The tumour size was determined by the fluorescent images using ImageJ programme. The experiment was repeated two times.

4.7. Statistical analysis

The experimental results were expressed as mean values ± SD. The differences in anti-angiogenic phenotypes between the untreated and treated groups were determined according to χ^2 test. In other tests, the differences between the untreated and treated groups, as well as between the treatments were evaluated using the one-way ANOVA followed by a comparison of the means by Bonferroni test (P = 0.05). All analyses were performed using SPSS 20 (SPSS Inc., Chicago, IL) software package.

Conflicts of interest

The authors declare that they have no known competing financial interests or personal relationships that could have appeared to influence the work reported in this paper.

Acknowledgements

Financial support from the Swiss National Science Foundation (project# 200021_196967, K. S. and F. Z.), the University of Fribourg and the Institute of Molecular Genetics and Genetic Engineering from the University of Belgrade (Ministry of Education, Science and Technological Development of the Republic of Serbia, 451-03-68/2022-14/200042) are gratefully acknowledged.

References

1 S. Ghosh, *Bioorg. Chem.*, 2019, **88**, 102925.
2 S. Su, Y. Chen, P. Zhang, R. Ma, W. Zhang, J. Liu, T. Li, H. Niu, Y. Cao, B. Hu, J. Gao, H. Sun, D. Fang, J. Wang, P. G. Wang, S. Xie, C. Wang and J. Ma, *Eur. J. Med. Chem.*, 2022, **243**, 114680.
3 S. Sen, M. Won, M. S. Levine, Y. Noh, A. C. Sedgwick, J. S. Kim, J. L. Sessler and J. F. Arambula, *Chem. Soc. Rev.*, 2022, **51**, 1212–1233.
4 R. Paprocka, M. Wiese-Szadkowska, S. Janciauskiene, T. Kosmalski, M. Kulik and A. Helmin-Basa, *Coord. Chem. Rev.*, 2022, **452**, 214307.
5 Z.-Y. Li, Q.-H. Shen, Z.-W. Mao and C.-P. Tan, *Chem. – Asian J.*, 2022, **17**, e202200270.
6 K. Schindler and F. Zobi, *Molecules*, 2022, **27**, 539.
7 Z. Huang and J. J. Wilson, *Eur. J. Inorg. Chem.*, 2021, **2021**, 1312–1324.
8 M. Mkhatshwa, J. M. Moremi, K. Makgopa and A.-L. E. Manicum, *Int. J. Mol. Sci.*, 2021, **22**, 6546.
9 H. S. Liew, C.-W. Mai, M. Zulkefeli, T. Madheswaran, L. V. Kiew, N. Delsuc and M. L. Low, *Molecules*, 2020, **25**, 4176.
10 P. Collery, D. Desmaele and V. Vijaykumar, *Curr. Pharm. Des.*, 2019, **25**, 1–17.
11 E. B. Bauer, A. A. Haase, R. M. Reich, D. C. Crans and F. E. Kühn, *Coord. Chem. Rev.*, 2019, **393**, 79–117.
12 C. C. Konkankit, S. C. Marker, K. M. Knopf and J. J. Wilson, *Dalton Trans.*, 2018, **47**, 9934–9974.
13 L. C. Lee, K. K. Leung and K. K. Lo, *Dalton Trans.*, 2017, **46**, 16357–16380.
14 A. Leonidova and G. Gasser, *ACS Chem. Biol.*, 2014, **9**, 2180–2193.
15 S. Ajay Sharma, N. Vaibhavi, B. Kar, U. Das and P. Paira, *RSC Adv.*, 2022, **12**, 20264–20295.
16 A. J. Amoroso, M. P. Coogan, J. E. Dunne, V. Fernández-Moreira, J. B. Hess, A. J. Hayes, D. Lloyd, C. Millet, S. J. A. Pope and C. Williams, *Chem. Commun.*, 2007, 3066–3068, DOI: 10.1039/B706657K.
17 M.-W. Louie, M. Ho-Chuen Lam and K. Kam-Wing Lo, *Eur. J. Inorg. Chem.*, 2009, **2009**, 4265–4273.
18 A. Leonidova, V. Pierroz, L. A. Adams, N. Barlow, S. Ferrari, B. Graham and G. Gasser, *ACS Med. Chem. Lett.*, 2014, **5**, 809–814.
19 R. R. Ye, C. P. Tan, M. H. Chen, L. Hao, L. N. Ji and Z. W. Mao, *Chem. – Eur. J.*, 2016, **22**, 7800–7809.
20 S. Clede, F. Lambert, R. Saint-Fort, M. A. Plamont, H. Bertrand, A. Vessieres and C. Policar, *Chem. – Eur. J.*, 2014, **20**, 8714–8722.
21 I. Kitanovic, S. Z. Can, H. Alborzinia, A. Kitanovic, V. Pierroz, A. Leonidova, A. Pinto, B. Spingler, S. Ferrari, R. Molteni, A. Steffen, N. Metzler-Nolte, S. Wolfl and G. Gasser, *Chem. – Eur. J.*, 2014, **20**, 2496–2507.
22 K. M. Knopf, B. L. Murphy, S. N. MacMillan, J. M. Baskin, M. P. Barr, E. Boros and J. J. Wilson, *J. Am. Chem. Soc.*, 2017, **139**, 14302–14314.
23 M. König, D. Siegmund, L. J. Raszeja, A. Prokop and N. Metzler-Nolte, *Med. Chem. Commun.*, 2018, **9**, 173–180.
24 C. C. Konkankit, A. P. King, K. M. Knopf, T. L. Southard and J. J. Wilson, *ACS Med. Chem. Lett.*, 2019, **10**, 822–827.
25 F. X. Wang, J. H. Liang, H. Zhang, Z. H. Wang, Q. Wan, C. P. Tan, L. N. Ji and Z. W. Mao, *ACS Appl. Mater. Interfaces*, 2019, **11**, 13123–13133.
26 M. Munoz-Osses, F. Godoy, A. Fierro, A. Gomez and N. Metzler-Nolte, *Dalton Trans.*, 2018, **47**, 1233–1242.
27 C.-C. Pagoni, V.-S. Xylouri, G. C. Kaiafas, M. Lazou, G. Bompola, E. Tsoukas, L. C. Papadopoulou, G. Psomas and D. Papagiannopoulou, *J. Biol. Inorg. Chem.*, 2019, **24**, 609–619.
28 M. Kaplanis, G. Stamatakis, V. D. Papakonstantinou, M. Paravatou-Petsotas, C. A. Demopoulos and C. A. Mitsopoulou, *J. Inorg. Biochem.*, 2014, **135**, 1–9.
29 G. Balakrishnan, T. Rajendran, K. Senthil Murugan, M. Sathish Kumar, V. K. Sivasubramanian, M. Ganesan,

A. Mahesh, T. Thirunalasundari and S. Rajagopal, *Inorg. Chim. Acta*, 2015, **434**, 51–59.
30 F. Zobi, B. Spingler and R. Alberto, *ChemBioChem*, 2005, **6**, 1397–1405.
31 A. P. King, S. C. Marker, R. V. Swanda, J. J. Woods, S.-B. Qian and J. J. Wilson, *Chem. – Eur. J.*, 2019, **25**, 9206–9210.
32 C. C. Konkankit, J. Lovett, H. H. Harris and J. J. Wilson, *Chem. Commun.*, 2020, **56**, 6515–6518.
33 S. C. Marker, A. P. King, S. Granja, B. Vaughn, J. J. Woods, E. Boros and J. J. Wilson, *Inorg. Chem.*, 2020, **59**, 10285–10303.
34 P. Collery, G. Bastian, F. Santoni, A. Mohsen, M. Wei, T. Collery, A. Tomas, D. Desmaele and J. D'Angelo, *Anticancer Res.*, 2014, **34**, 1679–1689.
35 P. Collery, A. Mohsen, A. Kermagoret, S. Corre, G. Bastian, A. Tomas, M. Wei, F. Santoni, N. Guerra, D. Desmaele and J. d'Angelo, *Invest. New Drugs*, 2015, **33**, 848–860.
36 V. Veena, A. Harikrishnan, B. Lakshmi, S. Khanna, D. Desmaele and P. Collery, *Anticancer Res.*, 2020, **40**, 1915–1920.
37 P. Collery, V. Veena, A. Harikrishnan and D. Desmaele, *Invest. New Drugs*, 2019, **37**, 973–983.
38 P. V. Simpson, I. Casari, S. Paternoster, B. W. Skelton, M. Falasca and M. Massi, *Chem. – Eur. J.*, 2017, **23**, 6518–6521.
39 A. Domenichini, I. Casari, P. V. Simpson, N. M. Desai, L. Chen, C. Dustin, J. S. Edmands, A. van der Vliet, M. Mohammadi, M. Massi and M. Falasca, *J. Exp. Clin. Cancer Res.*, 2020, **39**, 276.
40 S. N. Sovari, N. Radakovic, P. Roch, A. Crochet, A. Pavic and F. Zobi, *Eur. J. Med. Chem.*, 2021, **226**, 113858.
41 J. Rossier, D. Hauser, E. Kottelat, B. Rothen-Rutishauser and F. Zobi, *Dalton Trans.*, 2017, **46**, 2159–2164.
42 J. Delasoie, A. Pavic, N. Voutier, S. Vojnovic, A. Crochet, J. Nikodinovic-Runic and F. Zobi, *Eur. J. Med. Chem.*, 2020, **204**, 112583.
43 J. K. Stille, *Angew. Chem., Int. Ed. Engl.*, 1986, **25**, 508–524.
44 F. Zobi, *Inorg. Chem.*, 2009, **48**, 10845–10855.
45 E. Kottelat, F. Lucarini, A. Crochet, A. Ruggi and F. Zobi, *Eur. J. Inorg. Chem.*, 2019, **2019**, 3758–3768.
46 G. Schanne, L. Henry, H. C. Ong, A. Somogyi, K. Medjoubi, N. Delsuc, C. Policar, F. García and H. C. Bertrand, *Inorg. Chem. Front.*, 2021, **8**, 3905–3915.
47 L. D. Ramos, G. Cerchiaro and K. P. Morelli Frin, *Inorg. Chim. Acta*, 2020, **501**, 119329.
48 S. Clede, C. Sandt, P. Dumas and C. Policar, *Appl. Spectrosc.*, 2020, **74**, 63–71.
49 C. C. Konkankit, B. A. Vaughn, Z. Huang, E. Boros and J. J. Wilson, *Dalton Trans.*, 2020, **49**, 16062–16066.
50 L. D. Ramos, L. H. de Macedo, N. R. S. Gobo, K. T. de Oliveira, G. Cerchiaro and K. P. Morelli Frin, *Dalton Trans.*, 2020, **49**, 16154–16165.
51 P. T. Wilder, D. J. Weber, A. Winstead, S. Parnell, T. V. Hinton, M. Stevenson, D. Giri, S. Azemati, P. Olczak, B. V. Powell, T. Odebode, S. Tadesse, Y. Zhang, S. K. Pramanik, J. M. Wachira, S. Ghimire, P. McCarthy, A. Barfield, H. N. Banerjee, C. Chen, J. A. Golen, A. L. Rheingold, J. A. Krause, D. M. Ho, P. Y. Zavalij, R. Shaw and S. K. Mandal, *Mol. Cell. Biochem.*, 2018, **441**, 151–163.
52 P. A. Clarke, T. Roe, K. Swabey, S. M. Hobbs, C. McAndrew, K. Tomlin, I. Westwood, R. Burke, R. van Montfort and P. Workman, *Oncogene*, 2019, **38**, 5076–5090.
53 H. Shen, R. E. Perez, B. Davaadelger and C. G. Maki, *PLoS One*, 2013, **8**, e59848.
54 A. A. Untereiner, A. Pavlidou, N. Druzhyna, A. Papapetropoulos, M. R. Hellmich and C. Szabo, *Biochem. Pharmacol.*, 2018, **149**, 174–185.
55 P. M. De Angelis, K. L. Kravik, S. H. Tunheim, T. Haug and W. H. Reichelt, *Mol. Cancer*, 2004, **3**, 11.
56 R. Fior, V. Póvoa, R. V. Mendes, T. Carvalho, A. Gomes, N. Figueiredo and M. G. Ferreira, *Proc. Natl. Acad. Sci. U. S. A.*, 2017, **114**, E8234–E8243.
57 K. Kai, O. Nagano, E. Sugihara, Y. Arima, O. Sampetrean, T. Ishimoto, M. Nakanishi, N. T. Ueno, H. Iwase and H. Saya, *Cancer Sci.*, 2009, **100**, 2275–2282.
58 M. Tavares Barroso, B. Costa, C. Rebelo de Almeida, M. Castillo Martin, N. Couto, T. Carvalho and R. Fior, *Cells*, 2021, **10**, 2077.
59 R. White, K. Rose and L. Zon, *Nat. Rev. Cancer*, 2013, **13**, 624–636.
60 F. Zobi, B. Spingler and R. Alberto, *Dalton Trans.*, 2005, 2859–2865, DOI: **10.1039/b503874j**.
61 G. M. Sheldrick, *Acta Crystallogr., Sect. C: Struct. Chem.*, 2015, **71**, 3–8.
62 G. M. Sheldrick, *Acta Crystallogr., Sect. A: Found. Adv.*, 2015, **71**, 3–8.
63 C. Gütz and A. Lützen, *Synthesis*, 2010, 85–90.
64 T. Norrby, A. Borje, L. Zhang and B. Akermark, *Acta Chem. Scand.*, 1998, **52**, 77–85.
65 N. C. Fletcher, M. Nieuwenhuyzen and S. Rainey, *J. Chem. Soc., Dalton Trans.*, 2001, 2641–2648, DOI: **10.1039/B104365J**.
66 L.-Y. Liao, X.-R. Kong and X.-F. Duan, *J. Org. Chem.*, 2014, **79**, 777–782.
67 B. Imperiali, T. J. Prins and S. L. Fisher, *J. Org. Chem.*, 1993, **58**, 1613–1616.
68 J. Uenishi, T. Tanaka, K. Nishiwaki, S. Wakabayashi, S. Oae and H. Tsukube, *J. Org. Chem.*, 1993, **58**, 4382–4388.
69 S. A. Savage, A. P. Smith and C. L. Fraser, *J. Org. Chem.*, 1998, **63**, 10048–10051.
70 G. R. Newkome, W. E. Puckett, G. E. Kiefer, V. D. Gupta, Y. Xia, M. Coreil and M. A. Hackney, *J. Org. Chem.*, 1982, **47**, 4116–4120.
71 M. B. Hansen, S. E. Nielsen and K. Berg, *J. Immunol. Methods*, 1989, **119**, 203–210.
72 OECD, OECD, 2013, DOI: **10.1787/9789264203709-en**.
73 C. Zhao, X. Wang, Y. Zhao, Z. Li, S. Lin, Y. Wei and H. Yang, *PLoS One*, 2011, **6**, e21768–e21768.